

This dissertation/thesis/report entitled:

written by:

has been approved for the degree of:

in

by

1 - Advisor Name

2 - Department Chair or Committee Member Name

3 - Committee Member Name

4- Committee Member Name

5 - Committee Member Name

6 - Committee Member Name

Month YEAR



**Product and Catalyst Recovery for Aromatization of Palmitic Acid  
in the Presence of Supercritical Water**

by

Philip Smolitsky

A Thesis

Submitted to the Faculty

of the

WORCESTER POLYTECHNIC INSTITUTE

In partial fulfillment of the requirements for the

Degree of Master of Science

In

Chemical Engineering

by

---

August 2021

APPROVED:

---

Professor Michael Timko, Major Thesis Advisor

# Product and Catalyst Recovery for Aromatization of Palmitic Acid in the Presence of Supercritical Water

*Philip Smolitsky, Joseph P. Esposito, Jeffrey R. Page, Douglas P. Theberge, Azadeh Zaker,  
Siwen Wang, Sanket Sabnis, Wei Fan, Jesse Bond, Michael T. Timko*

A thesis submitted in partial fulfillment for the

degree of Master of Science

in

Chemical Engineering

August 2021

APPROVED:

---

Professor Aaron Deskins

---

Professor Nikolaos Kazantzis

---

Professor Andrew Teixeira

**Abstract:** Catalytic cracking of palmitic acid provides a renewable method of obtaining valuable aromatic compounds that are otherwise sourced from petroleum. In this study, ZSM-5 was evaluated for chemical production in a reaction mixture of palmitic acid and water at conditions near the critical point of water. The effects of ZSM-5 versus a nano-scale version of the catalyst, varying water loading amounts, product distribution and time dependence, catalyst reuse, and reaction pathway were studied. Nano-scale ZSM-5 with 15 wt% water loading provided the best aromatic yield, which was nearly double the next best aromatic producing reaction conditions. Catalyst was used four times, with some activity loss observed between the first and second cycle, and retention of activity for subsequent cycles. Used catalysts were also characterized for crystallinity, surface area, and acid properties, all of which were consistent with reuse tests. Time studies and control experiments suggest cooperative effects between thermal and catalytic reaction pathways.

## Introduction

Renewable alternatives to petroleum are a necessity for de-carbonizing the economy [1]. Most of the focus in this endeavor has been on the production of liquid fuels [2], but transitioning to a fully sustainable economy requires replacing petroleum-based chemicals with ones produced using renewable sources, as well [3,4]. As a matter of fact, chemicals are more valuable than fuels, so replacing petroleum chemicals with ones that are renewably sourced can potentially serve as a bridging technology to a decarbonized economy [5].

One of the most categories of industrial chemicals are the “BTEX” compounds, benzene, toluene, ethylbenzene, and xylene. These compounds are used for solvents, dyes, paints, and

plastic applications, which are all more valuable than fuels [6]. For this reason, using renewable sources to produce BTEX compounds can be economically viable in the short-term and provide a foundational plan for complete de-carbonization of the economy in the future [7].

Thermally cracking oils produces primarily fuels, with only small amounts of other chemicals. Gudiyella et al. [8] reported thermal conversion of vacuum residue to produce primarily diesel-range fuels, with several percent of BTEX compounds being co-produced. Catalytic cracking has been shown to increase chemical production, especially in the BTEX family [9-15]. Fatty acids recovered from waste cooking oils or algae are especially attractive feeds [11]. In addition, zeolites, specifically ZSM-5, have been proposed by several researchers for this purpose due to their selectivity towards single-ring aromatics [9-15]. However, coke accumulation causes zeolites used in fatty acid cracking to rapidly deactivate, hindering their use in commercial applications [16-19].

Recent work has shown the presence of water in a liquid or dense supercritical phase inhibits coke formation on ZSM-5. Zaker et al. [20] found that adding water to a reaction mixture containing dodecane in equal mass fractions decreased coke formation on ZSM-5 by more than 10 times relative to that observed in the absence of water. Similarly, Guerra et al. [21] reported that water inhibited conversion of single-ring aromatics to form multi-ring molecules associated with hard coke. This finding was attributed to water interfering with conversion of the methylbenzenium carbocation into hard coke.

In a separate study, Zaker et al. [22] performed a reaction engineering analysis of ZSM-5 catalyzed dodecane cracking in the presence and absence of water near its supercritical state, and found that a carbocation-based mechanism of cracking and aromatization accounted for experimental observations of conversion and product distribution. Water decreased the rate

constants used to describe dodecane cracking and especially coke formation, with less impact on aromatization rate constants. In addition, water opened new pathways of low-temperature hydrocarbon reformation and coke gasification that prevented coke accumulation on the surface. Accordingly, water interrupts carbocation coke formation pathways [21] as well as opens new pathways for coke removal [22].

Using supercritical water to control coke formation on zeolites used for chemical production from waste oils presents two problems. The first problem is that water promotes zeolite decrystallization and dealumination, which leads to irreversible activity loss [23-25]. Previous reports on the reuse of zeolites in the presence of liquid water have yielded mixed results [24-27]. The second problem that arises is that oil cracking in zeolites at typical conditions ( $>350$  °C) is likely diffusion limited [22, 28, 29], and diffusion limited reactions contribute to coke formation and catalyst deactivation [30]. Nanoscale zeolites, or other approaches to decrease diffusion path lengths, have shown promise for promoting cracking activity while decreasing coke formation [31]. In fact, nanoscale zeolites and secondary water components may be mutually beneficial for maximizing activity, reducing coke formation, and improving catalyst reuse.

The use of nano-scale zeolites and supercritical co-feeding with a non-polar reactant have not been evaluated for conversion of fatty acids to BTEX chemicals. Instead, zeolite-catalyzed aromatization studies in the presence of supercritical water component utilize microscale zeolites and co-feed of  $>50$  wt% water with the fatty acid [27, 32, 33]. As a result, the previously mentioned questions about coke inhibition, zeolite degradation, and reaction mechanism remain unanswered. Answering these questions is important to advance the field and potentially open new avenues for study that involve residual – rather than dominant – water c-feed.

In this study, we evaluate ZSM-5 catalyzed palmitic acid cracking in the presence of water under single fluid phase conditions near the critical point of water, 400 °C and 22±2 MPa, in a batch reactor. Palmitic acid was selected as a model reactant because of its abundance in used cooking oil and microalgae [19, 34, 35]. ZSM-5 was selected as a commercial zeolite with known BTEX formation activity and with greater stability in the presence of liquid water than other commercial zeolites [25]. Reaction conditions were selected to ensure that palmitic acid, water, and primary reaction products formed a thermodynamically stable single phase, which would eliminate uncertainty stemming from fluid-fluid interfaces [36]. The effects of using ZSM-5 versus a nano-scale version of the catalyst and varying water loading amounts in the reaction mixture were tested. Additionally, catalyst activity, selectivity, and reuse were examined and compared with previous reports on palmitic acid cracking in the presence and absence of water in the reaction mixture. Catalyst reuse tests were performed and used catalysts were characterized for signs of degradation. Lastly, time study data and comparison with product distributions obtained under thermal conditions were used to propose a possible thermos-catalytic mechanism. These results suggest water as a new strategy for managing catalyst deactivation while still converting renewable and waste oil feeds into valuable chemicals.

## **Methodology**

### **Materials**

Palmitic Acid with a purity of 98% was acquired from Acros Organics (p/n AC1297000010). ZSM-5 was obtained from ACS materials with a silica-to-alumina atomic ratio of 117. Nano-HZSM was obtained from ACS materials with a silica-to alumina atomic ratio of 26. Fresh catalyst was dried in an oven at 100 °C for 3 h before being calcined (550 °C for 15 h) to

remove template material. Water was de-ionized to a minimum resistivity of 17.9 M $\Omega$ -cm immediately prior to use. ACS reagent grade dichloromethane (CH<sub>2</sub>Cl<sub>2</sub>, DCM) was obtained from Pharmco-AAPER at 99.8% purity. ACS reagent grade acetone (C<sub>3</sub>H<sub>6</sub>O) was obtained from Fisher chemical at 99.5% purity. n-heptane (C<sub>7</sub>H<sub>16</sub>) was obtained from Acros Organics at 99+% purity. HPLC grade methanol was obtained from Sigma-Aldrich at 99.9% purity. D-chloroform was purchased from Cambridge Isotope Labs (p/n DLM-7TB-100S) with a purity of 99.8% and a TMS of 0.05%. Compressed nitrogen, helium, hydrogen and air (99.999% purity) were obtained from Airgas.

### **Reaction Protocol**

Reactions were conducted in a 100 cm<sup>3</sup> stainless steel Parr batch reactor (p/n 4590 micro) equipped with gas inlet and release valves, a 0–35 MPa pressure gauge (p/n 593HCP50AD) and a rupture disk (p/n 526HCP50CTYZ50) for safety. A Parr magnetic drive (p/n A1120HC6) and stainless-steel stirring rod were used to control mixing within the reactor. An electric heating jacket (Parr Instrument, p/n A3240HC6EB) was used to heat the reactor to a desired temperature based on readings from a thermocouple (p/n A472E2) within the reactor. Temperature and stirring rate were set using a reactor controller (Parr Instrument, p/n 4848).

For all reactions, 8.00 grams of palmitic acid (PA) and 0.40 grams of either ZSM-5 or nano ZSM-5 (5 wt% relative to the initial PA loading) were placed in the reactor. Then either 1.41 grams (15 wt%) or 15.0 grams (65 wt%) of DI water were added into the reactor, or water was excluded from the reaction. After loading reactants, nitrogen gas was fed to the reactor (~3.4 MPa) and vented at least five times to purge it of air prior to reaction. For reactions with either 1.41 grams of water or no water, the reactor was pressurized to 9 MPa with nitrogen gas. For reactions with 15.0 grams of water, the reactor was pressurized to 5 MPa. This was done to ensure the reaction

reached supercritical pressure ( $23 \pm 1$  MPa) and heated to the desired temperature (for most reactions  $400$  °C). The reaction temperature was held for a specified duration ranging from 0 to 90 minutes, after which the reactor was removed from the heater and quenched in a water bath. All experiments were carried out at least twice to evaluate reproducibility.

Catalyst re-use experiments were conducted for the 30-minute reaction, since it was the shortest reaction to reach  $\sim 100\%$  conversion. Catalyst was collected from several 30-minute reactions and de-coked in air for 15 hours at  $550$  °C. Remaining catalyst was used to conduct a subsequent cracking reaction with the same conditions (30 minutes,  $400$  °C $\pm$ ,  $23\pm 1$  MPa, 15 wt% water, 5 wt% nano ZSM-5), and four re-use reactions were conducted. These re-use runs were labelled 'Fresh' for reactions with catalyst which had not been previously used, and 'Cycle X' for reactions with catalyst de-coked after X reactions. Each re-use cycle was conducted at least twice except for the final re-use cycle (due to depletion of catalyst) to ensure reproducibility of data.

## **Product Analysis**

After reaction, the gas collected in the reactor was vented through a gas chromatograph (GC) sample loop for quantification. The reactor was then opened, and the oil product recovered and analyzed by a separate GC and (for representative samples) proton nuclear magnetic resonance (NMR), as well as 2-dimensional GC to verify make-up of oil-phase products. Solids were removed by filtration and stored for further analysis.

During reactions, reactor temperature and pressure as well as reaction time were recorded. Experiments with procedural outliers (obvious gas leaks, slow temperature ramp, et cetera) were immediately disqualified for analysis. Reactor leaks were tested for before reactions by holding initial pressure of 9 MPa for 1-2 minutes, and after by weighing the gas-phase product.

Gas-phase products were analyzed with a GC (GC-2014 Shimadzu system) equipped with a thermal conductivity detector (TCD) an 80/100 Hayesep Q packed column (3 m × 0.125 in × 2.1 mm SS). The carrier gas was helium with a flow rate of 10 sccm. The initial temperature was 30 °C, and which was increased at rate of 5 °C min<sup>-1</sup> until reaching 90 °C, after which the temperature was held for 20 minutes. The TCD temperature was set to 150 °C and the current was set to 120 mA. Gases were identified by retention time matching with known standards and TCD response areas were converted into concentrations using calibrated response factors. Residence times and response factors were determined for the following compounds: CO<sub>2</sub>, CH<sub>4</sub>, C<sub>2</sub>H<sub>4</sub>, C<sub>2</sub>H<sub>6</sub>, C<sub>3</sub>H<sub>8</sub>, C<sub>4</sub>H<sub>10</sub>, C<sub>5</sub>H<sub>12</sub>, and C<sub>6</sub>H<sub>14</sub> using calibration standards. Different isomers of C<sub>4</sub> through C<sub>6</sub> compounds were unable to be distinguished, and for this reason the relative ratios of the isomers were assumed to be the same as the oil phase for analysis.

For analysis, the oil and water phases separated under gravity and the supernatant oil phase was filtered and diluted with DCM in a ratio of 1:100. This solution was analyzed using a GC equipped with a quadrupole mass spectrometer detector (MS, QP 2010 SE system, Shimadzu) for product identification and a flame ionization detection (FID, Shimadzu) for quantification.

For GC-MS, the column was SHRXI-5MS (30 m×0.25 mm ID×0.5 µm film thickness), and for FID the column was Rt-Q-BOND (30 m×0.25 mm ID×8 µm film thickness). The same temperature program was used for both FID and GC-MS: the initial column temperature was 35 °C and the column temperature increased at 3 °C min<sup>-1</sup> until reaching 290 °C, at which point the temperature was held constant for 5 minutes before completion. The injector temperature was 300 °C and the injected sample volume was 3 µl. FID response factors were determined using hexane, heptane, octane, decane, dodecane, hexadecane, toluene, o-xylene, ethylbenzene, 1,2,4-trimethylbenzene, 1-methylnaphthalene and palmitic acid and generalized using the method

described by Perkins et al. [37]. Yields were calculated on a mole and mass basis using FID areas, response factors, and initial PA loading.

GC analysis was able to quantify approximately 80-100% of the individual oil products formed after the PA reaction. To test for any unreacted PA in the oil phase, the oil was placed in a dish and dissolved in about 40 grams of DCM. Then a steady flow of nitrogen was allowed to flow over the dish so that the DCM could evaporate and strip the oil solution of products, leaving behind PA. The dish was weighed many times over the course of this process until the weight stabilized.

Solids were separated from the oil by vacuum filtration followed by washing the solids with water and DCM until the solvent passing through the filter was clear. Coke was then placed in a 60 °C oven overnight to remove excess DCM. The washed and dried solids were then placed in a ceramic boat and weighed before being placed in a quartz tube furnace. Airflow into the furnace was set to 2 mL min<sup>-1</sup> and the temperature was increased from ambient to 550 °C at a ramp rate of 10 °C min<sup>-1</sup>, at which point the sample was de-coked for 10 hours. Then the sample was removed and weighed to measure the amount of coke burned off and the amount of catalyst remaining.

### **Catalyst Analysis**

Catalyst characterization was performed using X-ray powder diffraction (XRD), Fourier Transform Infrared Spectrograph (FT-IR), N<sub>2</sub> adsorption isotherm analysis, and Scanning Electron Microscopy (SEM). The same catalyst used in the reuse experiments was used for catalyst characterization. The catalyst was de-coked before characterization following the same de-coking procedure outlined in the catalyst re-use experiments section above.

Diffuse Reflectance Infrared Fourier Transform Spectroscopy (DRIFT) was performed using a Nicolet Magna IR 560 spectrometer and a SpectraTech DRIFTS cell. This method was based on the DRIFTS method from Maag et al. [23]. The cell was loaded with ZSM-5 before being purged with N<sub>2</sub> for 10 minutes to remove ambient CO<sub>2</sub>. The temperature was increased in 20 °C increments at 10-15 min intervals until 100 °C, where it was held for 30 minutes before increasing in 50 °C increments until reaching 550 °C. Samples were analyzed over the range from 4000 to 600 cm<sup>-1</sup>, at a resolution of 2 cm<sup>-1</sup>, and an accumulation of 256 scans at 550 °C.

The X-Ray Powder Diffraction (XRD) patterns were taken using a Rigaku X-ray diffractometer with Cu K $\alpha$  radiation at 37.5 keV and 25 mA. A scan rate of 0.05° (2 $\theta$ ) per second over a 6 theta to 80 range was used. XRD patterns were analyzed using MDI Jade software. The degree of crystallinity was calculated using the ASTM Standard D5758 [46].

N<sub>2</sub> Adsorption was performed using a Quantachrome autosorb IQ to determine catalyst surface area and micropore volume. Zeolite samples (~0.1 g) were added to a glass bulb and degassed at a temperature ramp of 2 °C min<sup>-1</sup> with 30 min temperature holds at 80 and 120 °C before increasing to 350 °C for 420 min. Analysis was performed by dosing the sample with nitrogen as the adsorbate and cooling the sample with liquid nitrogen. 43 isothermal P/P<sub>0</sub> points were obtained between 0.00013 and 1 followed by 16 desorption points from 1 to 0.1. Micropore and external surface area were determined by applying the DR method to model the adsorption isotherm between P/P<sub>0</sub> of 0.15 to 0.95.

## **Results and Discussion**

The objective of this study was to examine the promotional effect of dense liquid water on the activity, re-use, and stability of ZSM-5 used for palmitic acid (PA) cracking. Most experiments

were performed at 400 °C and  $23 \pm 1$  MPa. While water as a pure substance would be in its supercritical state at the selected reaction conditions, as a mixture the supercritical state is no longer clearly defined thermodynamically [39]. At 400 °C and  $23 \pm 1$  MPa, water is present as a dense, liquid-like form that approximates its supercritical state [40]. Accordingly, water is described as being in its supercritical state, following standard convention [39].

The majority of this study consists of experimental measurements of cracking rates and product distribution, followed by re-use and zeolite characterization tests. Accordingly, the results are presented in three sections: 1) activity and product analysis tests, 2) catalyst stability and reuse testing, and 3) reaction pathway analysis.

### Activity and Product Analysis

Experiments were performed over a range of reaction times, including the time required for heat-up and reaction quenching (i.e., 0 min) and for subsequent reaction times to 90 min. Table 1 summarizes yields of all major products (i.e., any product with a molar yield greater than 0.05 relative to the initial moles of PA charged to the reactor), categorized as palmitic acid (PA), CO<sub>2</sub>, C<sub>1</sub>-C<sub>3</sub> gases, aliphatics, and aromatics. Complete speciation data are provided in Table SI-1 in the Supporting Information. As expected, PA conversion increases with increasing reaction time and reaction temperature. At 400 °C, PA was detected only when the reaction time was  $\leq 15$  min. For all other reaction times, PA concentrations in the product mixture were less than the detection limit and the corresponding conversion could only be estimated as  $>0.998$ . Accordingly, ZSM-5 catalyzed cracking of PA in the presence of water (15 wt%) is rapid and complete.

| Products<br>(mol/mol PA)             | 0 min, 350°C | 0 min, 400°C | 15 min,<br>400°C | 30 min,<br>400°C | 45 min,<br>400°C | 90 min,<br>400°C |
|--------------------------------------|--------------|--------------|------------------|------------------|------------------|------------------|
| CO <sub>2</sub>                      | 0.07 ± 0.03  | 0.03 ± 0.03  | 0.11 ± 0.04      | 0.12 ± 0.03      | 0.11 ± 0.04      | 0.08 ± 0.02      |
| Total C <sub>1</sub> -C <sub>3</sub> | 0.09 ± 0.04  | 0.06 ± 0.03  | 0.21 ± 0.07      | 0.24 ± 0.06      | 0.21 ± 0.05      | 0.24 ± 0.02      |

|                         |             |             |             |             |             |             |
|-------------------------|-------------|-------------|-------------|-------------|-------------|-------------|
| <b>C<sub>4</sub></b>    | 0.23 ± 0.04 | 0.42 ± 0.10 | 0.56 ± 0.22 | 0.58 ± 0.06 | 0.52 ± 0.12 | 0.47 ± 0.02 |
| <b>C<sub>5</sub></b>    | 0.26 ± 0.06 | 0.48 ± 0.07 | 0.52 ± 0.09 | 0.50 ± 0.04 | 0.50 ± 0.08 | 0.36 ± 0.02 |
| <b>C<sub>6</sub></b>    | 0.21 ± 0.16 | 0.22 ± 0.04 | 0.24 ± 0.05 | 0.21 ± 0.04 | 0.20 ± 0.05 | 0.16 ± 0.02 |
| <b>C<sub>7</sub></b>    | 0.06 ± 0.00 | 0.09 ± 0.01 | 0.08 ± 0.01 | 0.06 ± 0.01 | 0.07 ± 0.01 | 0.07 ± 0.01 |
| <b>C<sub>8</sub></b>    | 0.06 ± 0.01 | 0.07 ± 0.01 | 0.07 ± 0.01 | 0.06 ± 0.00 | 0.07 ± 0.00 | 0.06 ± 0.02 |
| <b>Total Aliphatics</b> | 0.86 ± 0.12 | 1.35 ± 0.15 | 1.54 ± 0.23 | 1.46 ± 0.08 | 1.39 ± 0.14 | 1.17 ± 0.02 |
| <b>Olefin/Paraffin</b>  | 1.32 ± 0.34 | 1.09 ± 0.12 | 1.03 ± 0.06 | 0.52 ± 0.10 | 0.65 ± 0.09 | 0.54 ± 0.17 |
| <b>Benzene</b>          | 0.01 ± 0.00 | 0.02 ± 0.00 | 0.02 ± 0.00 | 0.03 ± 0.00 | 0.03 ± 0.00 | 0.04 ± 0.01 |
| <b>Toluene</b>          | 0.06 ± 0.00 | 0.10 ± 0.01 | 0.11 ± 0.02 | 0.17 ± 0.01 | 0.14 ± 0.01 | 0.18 ± 0.03 |
| <b>Ethylbenzene</b>     | 0.02 ± 0.00 | 0.04 ± 0.00 | 0.04 ± 0.01 | 0.06 ± 0.00 | 0.05 ± 0.00 | 0.06 ± 0.01 |
| <b>Xylene</b>           | 0.10 ± 0.01 | 0.15 ± 0.01 | 0.17 ± 0.03 | 0.23 ± 0.01 | 0.21 ± 0.01 | 0.25 ± 0.03 |
| <b>Total Aromatics</b>  | 0.39 ± 0.06 | 0.63 ± 0.05 | 0.69 ± 0.11 | 0.91 ± 0.04 | 0.86 ± 0.05 | 1.06 ± 0.06 |
| <b>PA Conversion</b>    | 0.60 ± 0.01 | 0.92 ± 0.02 | 0.97 ± 0.02 | > 0.998     | > 0.998     | > 0.998     |

**Table 1.** Molar yield of products (mol of product per mol of palmitic acid) over a range of reaction durations and at several temperatures, all with 5 wt% ZSM-5 (relative to palmitic acid), 15 wt% water, and  $23 \pm 1$  MPa.

Product yields were monitored as a function of reaction time. CO<sub>2</sub> was a major product under most conditions and its yield generally increased with PA conversion. The major source of CO<sub>2</sub> is PA decarboxylation [27, 40]. CO could not be quantified separately; however, previous work by Class et al. [38] suggests that the majority of CO<sub>x</sub> products formed under the reaction conditions used here should be present as CO<sub>2</sub> due to the water-gas-shift reaction. Yields of C<sub>1</sub>-C<sub>3</sub> gases were similar to those observed for CO<sub>2</sub>.

Hydrocarbons were the primary reaction product at all times. Both paraffins and olefins were formed, and C<sub>4</sub> and C<sub>5</sub> compounds were the most abundant aliphatic products. This observation indicates rapid cracking of the C<sub>16</sub> carbon chain of palmitic acid into smaller fragments. The olefin-to-paraffin ratio generally decreased with increasing PA conversion,

consistent with olefin formation as a primary product of decarboxylation and PA cracking reactions followed by subsequent saturation or cyclization.

Aromatic yields increased over time, starting at  $0.63 \pm 0.05$  for the shortest reaction time and increasing to  $>1 \text{ mol mol}^{-1}$  after 90 min. Interestingly, aromatic yields continued to increase after PA conversion had reached completion, indicating formation of aromatic products by secondary reactions involving paraffins and/or olefins. Independent of PA conversion, toluene and xylene were the most abundant one-ring aromatics. In general, yields of two-ring aromatics were an order of magnitude less than the one-ring aromatics, as desired from an economic perspective.

Aside from the compounds shown in Table 1, coke and products too heavy to be analyzed using GC were also formed. Coke yields were measured at 30 min of reaction time at 400 °C with 15 wt% SCW as  $2.6 \text{ mg g}^{-1}$  PA, showing a ~4x reduction from a  $12.2 \text{ mg g}^{-1}$  PA coke yield without SCW measured from two reactions conducted at identical conditions without added water. Accordingly, coke formation occurred rapidly, consistent with a previous report by Zaker et al. [20]. Visually, the appearance of the recovered catalyst progresses from brown to black with increasing reaction time, consistent with its conversion from aliphatic soft coke to aromatic hard coke, as previously observed by Guerra et al. [21].

Heavy products were analyzed using  $^1\text{H-NMR}$  as a volatility-independent method to evaluate composition. Figure A1 in the appendix provides the raw  $^1\text{H-NMR}$  spectra. In summary,  $^1\text{H-NMR}$  indicates that the heavy products are composed of polycyclic aromatic hydrocarbons and/or aromatics bearing aliphatic side chains.

A major objective of this study was to determine the effects of a residual water and using ZSM-5 versus nano ZSM-5 on catalyzed fatty acid cracking. To evaluate this effect, the products of these cracking reactions were evaluated after reactions with each combination of water loading and catalyst type (nano ZSM-5 or commercial ZSM-5, and no water, 15 wt% water loading, or 65 wt% water loading). The distribution of product yields in these reactions are shown in Figure 1.

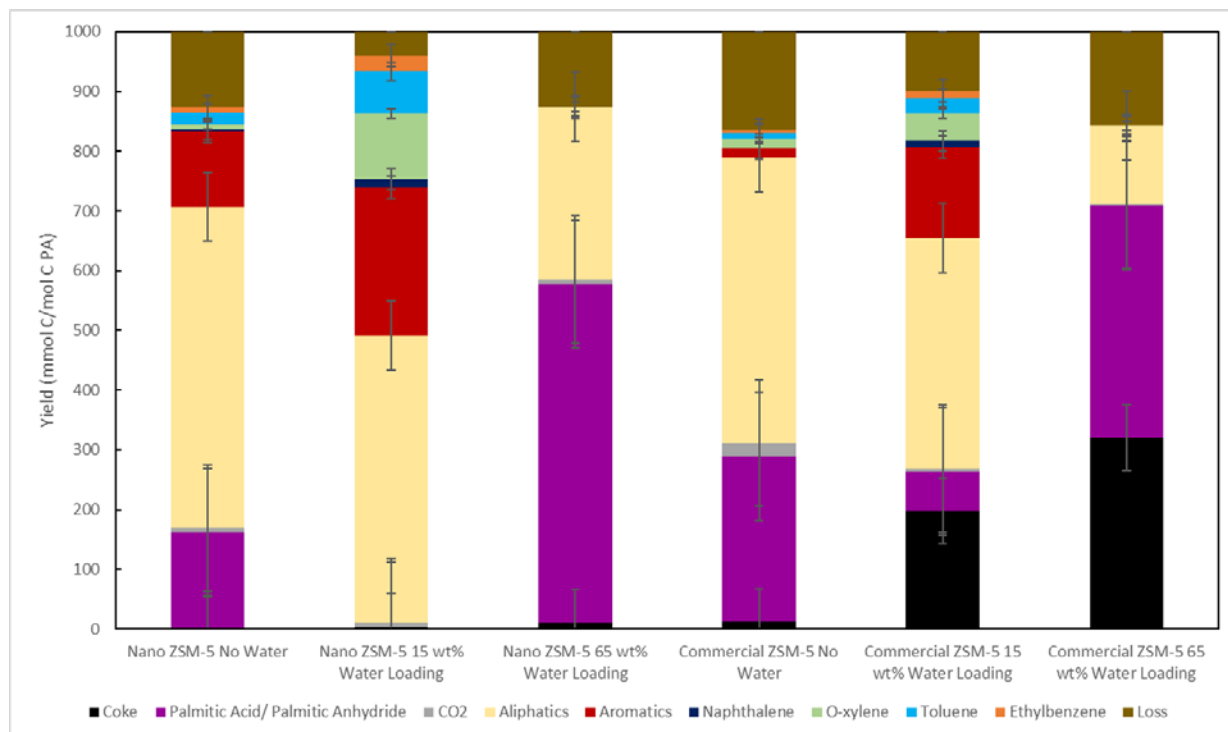
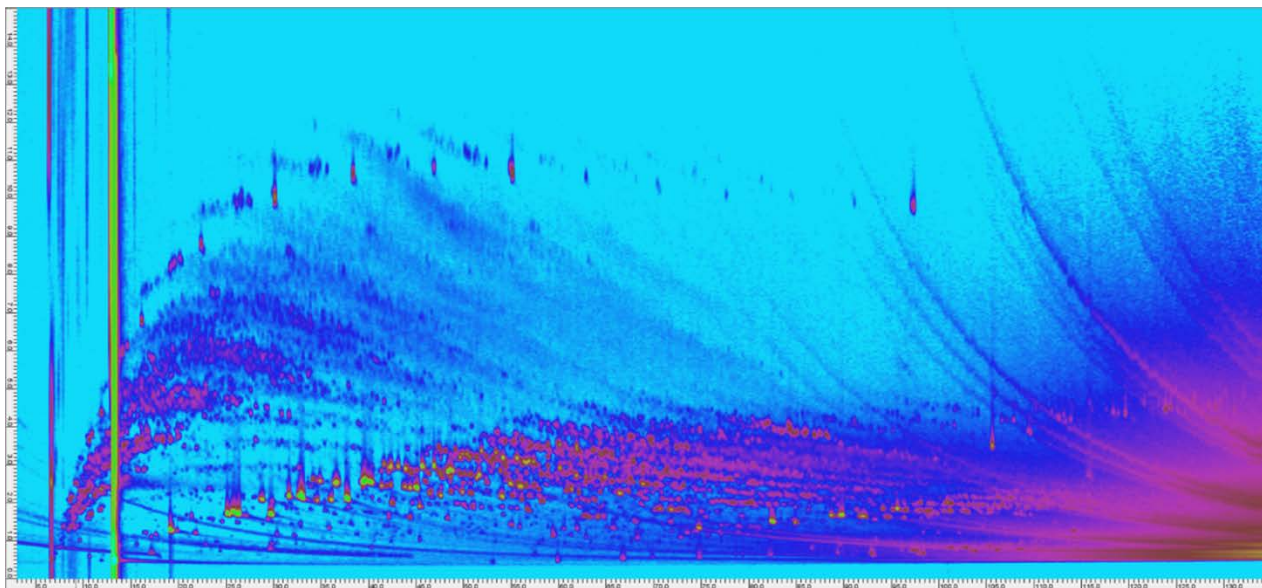


**Figure 1.** Product yields of reactions testing water loading and catalyst type combinations. Primary products, as well as coke produced and loss are shown.

The trends for both commercial and nano ZSM-5 are similar. Coke yield increased with the amount of water present in the reaction. When the water loading was 65 wt%, no aromatic production was observed for the reactions with commercial and nano ZSM-5. For both catalysts, the most aromatic production was observed when water loading was 15 wt%. For this case, commercial ZSM-5 produced about half of the BTEX compounds that nano ZSM-5 did, but still

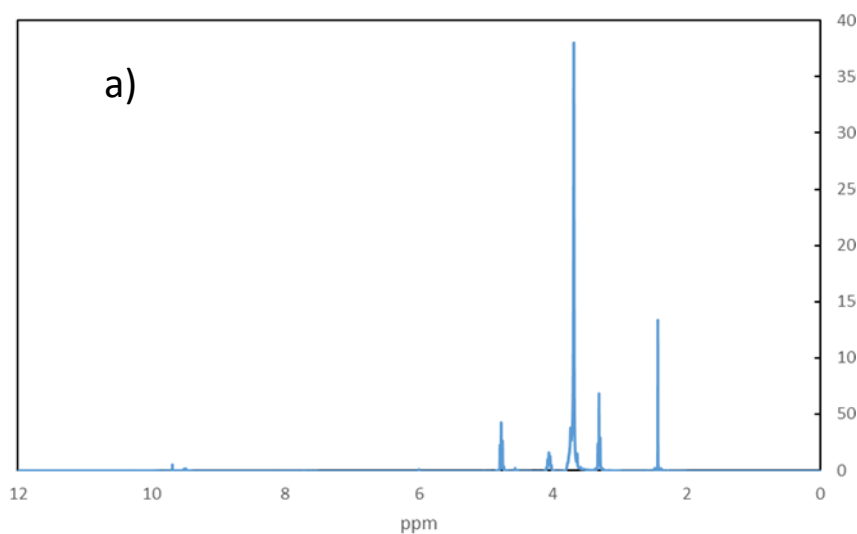
about three times more than the same catalyst with no water. After going through all the water loading and catalyst combinations, 15 wt% water loading and nano ZSM-5 was the best for the BTEX compound production that we were looking for, and especially with ~100% conversion and 47% aromatic yield.

Two dimensional gas chromatography (GCxGC) was also ran on an oil sample from a reaction containing 15 wt% water and nano ZSM-5. Since GC/MS can't differentiate between different isomers of compounds, GCxGC, which uses two separation columns to further separate compounds, can be utilized to create a clear visual representation of that differentiation. Figure 2 shows the GCxGC plot generated from a sample from a run using nano ZSM-5 and 15 wt% water. There is clear separation between aromatics and nonaromatic compounds, and those can be further separated into compounds such as paraffins, olefins, and alkyl- aromatics. GCxGC verifies the separation we observe using one-dimensional GC/MS, while also providing a bit more detail.



**Figure 2.** Two dimensional gas chromatograph (GCxGC) of the oil product from a reaction containing 15 wt% water loading and nano ZSM-5.

For the 65 wt% water loading reactions, there was a large amount of white solid removed from the reactor when product collection took place. It was assumed that this was unreacted palmitic acid at first, but when it didn't dissolve in DCM like the other samples, it became apparent that this wasn't the case. It was hypothesized that this was actually palmitic anhydride that was formed during the reaction. This was tested by running H-NMR spectroscopy of this white solid sample, as well as a known sample of pure palmitic anhydride. The NMR spectra of these are shown in figure 3. Due to the similarity of the spectra for each sample, it was concluded that this solid product was, in fact, palmitic anhydride, and was reported as such for the 65 wt% water loading reactions.



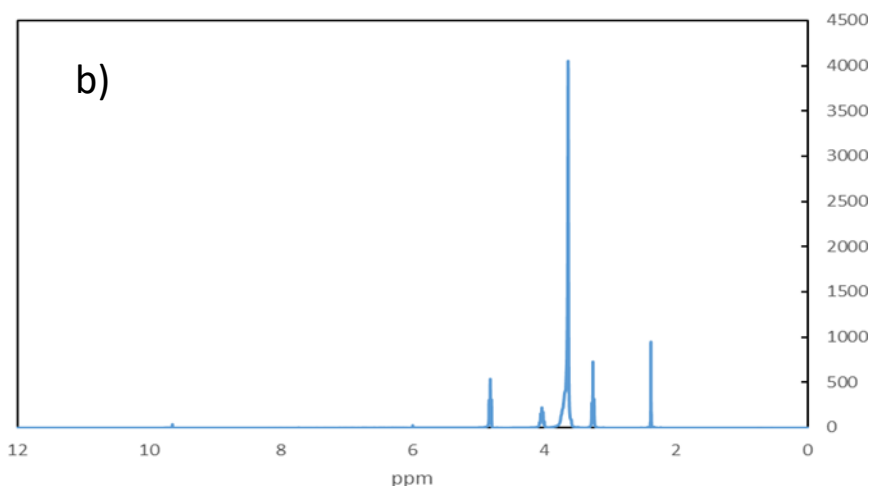


**Figure 3.** H-NMR spectra of a) the solid sample removed from a 65 wt% water loading reaction and b) pure palmitic anhydride.

The overall results produced can be compared to several data sets measured at similar conditions [9, 10, 12, 14, 27]. Table 2 summarizes this comparison.

| Reference         | Feed         | Reaction Conditions<br>(Temp / Pres / Time) | Cat.<br>Loading<br>(g/g PA) | Water<br>Loading<br>(wt%) | Conversion<br>(%) | Coke<br>Yield<br>(wt%) | Aromatic<br>Selectivity     |
|-------------------|--------------|---|-----------------------------|---------------------------|-------------------|------------------------|-----------------------------|
| <b>This Work</b>  | <b>PA</b>    | <b>400°C / &gt;22.1 MPa / 30 min</b>        | <b>0.05</b>                 | <b>15</b>                 | <b>~100</b>       | <b>0.29</b>            | <b>63 wt%<br/>(47 mol%)</b> |
| Mo et al.         | PA           | 400 °C / >24 MPa / 25 min                   | 1.00                        | 66                        | 43                | NR <sup>a</sup>        | 39 mol%                     |
| Emori et al.      | Soybean Oil  | 450°C / 0.1 MPa / 45 min                    | 0.33                        | 0                         | ~100              | NR <sup>a</sup>        | 22-40 wt%                   |
| Katikaneni et al. | Canola Oil   | 400°C / 0.1 MPa / 30 min                    | 1.11                        | 25                        | 93                | 2.0                    | 41 wt%                      |
|                   |              | 400°C / 0.1 MPa / 30 min                    | 0.56                        | 25                        | 92                | 3.0                    | 42 wt%                      |
| Botas et al.      | Rapeseed Oil | 550°C / 0.1 MPa / 60 min                    | 0.13                        | 0                         | ~100              | -                      | 34 wt%                      |
| Twaiq et al.      | Palm Oil     | 400°C / 0.1 MPa / n/a                       | 0.40                        | 0                         | 97                | 1.7                    | 38 wt%                      |

<sup>a</sup> NR denotes “not reported”

**Table 2.** Comparison of values from 15 wt% water loading with to values from other fatty acid cracking studies with ZSM-5 [9, 10, 12, 14, 27].

The most direct comparison with the current data set is with the study reported by Mo et al.;[27] the main difference between the two studies is the initial water loadings used in the two studies (66 wt% in Mo et al. [27] compared with 15 wt% in the current study). Interestingly, after accounting for differences in PA conversion and catalyst loading, the estimated reaction rate observed in the current study is 65-times greater than that reported by Mo et al. [27]. The aromatic selectivity was also higher than what Mo et al. reported (47 vs. 39 mol%). Accordingly, reducing initial water loading increases PA cracking rates without sacrificing aromatic selectivity. Although Mo et al. [27] did not report coke yields, the coke yield observed here (<1 wt%) is a fraction of what has been reported previously for catalytic fatty acid cracking studies [12, 14].

In addition to the comparison with the study reported by Mo et al. [27], Table 2 provides several other useful comparisons with fatty acid cracking catalyzed by ZSM-5 at atmospheric pressure. While studies at atmospheric pressure evaluated more complex feeds than PA, which prevents direct comparison,, Table 2 shows that supercritical water decreases coke formation without sacrificing reaction rate or aromatic selectivity.

All of these considerations indicate that fatty acid cracking in the presence of a minority water component confers the coke reduction benefits of supercritical water, while increasing cracking rates and without sacrificing aromatic yields. Previous work on the use of catalysts in the presence of supercritical water has reported mixed results on catalyst lifetime, and regenerability [27]. Accordingly, the next step of this study was testing catalyst reusability.

### **Catalyst Stability and Reuse**

To test the reusability of the ZSM-5 catalyst, a sequence of reactions was performed at standard conditions (30 minutes at 400°C). Catalyst was recovered after each reaction, regenerated

by removing coke, and reused. In total, catalyst activity was evaluated for 4 cycles. Of all of the products, aromatic yields are the best indicator of catalyst performance after regeneration. Accordingly, Figure 3 provides aromatic yields and selectivity observed for each of the 4 cycles. All experiments were performed at least in duplicate, with error bars shown, except for cycle 3, which was performed only once. Based on the uncertainties of the rest of the data, the uncertainty in yields obtained after cycle 3 are <5%.

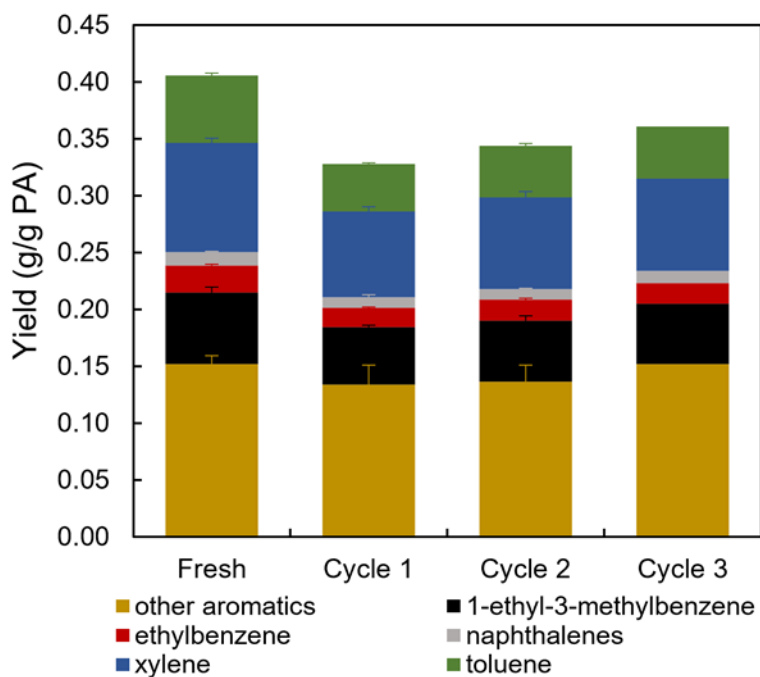


**Figure 3.** Comparison of aromatic yield between cycles of catalyst use. Catalyst was de-coked after use for 15 hours in air. Reactions are labeled by the catalyst used for the reaction, for example ‘Fresh’ was used in the initial reaction. Once used and de-coked, this ‘Fresh’ catalyst is called ‘Cycle 1.’ The same pattern is continued for Cycle 2 and Cycle 3. Reaction conditions: 30-minutes, 400°C, and  $23 \pm 1$  MPa.

Figure 3 shows that aromatic yield decreases after first catalyst reuse by approximately 20%, with aromatic yield then gradually increases with each successive use. Cycle 3 retains 88%

of the aromatic yield observed for the fresh catalyst. For comparison, previous studies with more abundant water components in the reaction mixture report that aromatic yield decreased by 40% after three use-reuse cycles [27].

Activity tests shown in Figure 3 provide a strong indication of the reusability of ZSM-5 under the current reaction conditions. To further explore this, the used catalysts were recovered and evaluated for signs of degradation using x-ray diffraction (XRD) to monitor changes in crystallinity, N<sub>2</sub> sorption to study texture properties, and infrared (IR) spectroscopy to evaluate chemical changes.

Zeolite crystallinity retention is a common way to quantify degradation in hot liquid and supercritical water.[45, 46] In particular, Zaker et al.[20] showed that retention of crystallinity was required for retention of zeolite activity. Representative XRD patterns for each reuse cycle can be seen in Figure 4. The sharp diffraction peaks from 23-25 2 $\theta$  degrees associated with the MFI framework of ZSM-5 are visible after every cycle, suggesting that crystalline structure is at least partially retained after four cycles of use. Moreover, no new peaks appear after use, indicating that no new crystalline phases form at reaction conditions.

To quantify the crystallinity change, ASTM Standard D5758 [47] was used to integrate the area under the XRD curve and compared with the value obtained for the fresh catalyst. This standard has been found to be reproducible within 3% and has a 95% confidence interval of  $\pm 5.04\%$  [47]. Crystallinity values are provided directly in Figure 3 for reference. In all cases, ZSM-5 retained  $\geq 90\%$  of its initial crystallinity, with most of the change occurring between the first and second use. After the initial decrease, crystallinity reaches a stable value of approximately 90%. This suggests that ZSM-5 may consist of some regions that are vulnerable to amorphization. Once these are removed, the remaining material is stable to further amorphization.

In comparison with the results obtained from using ZSM-5 in the presence of a minority water component (15 wt%), Zaker et al.[20] reported that the crystallinity of ZSM-5 used in a reaction mixture containing 50 wt% water decreased by >20% after a single use, establishing that the current conditions are much less aggressive.

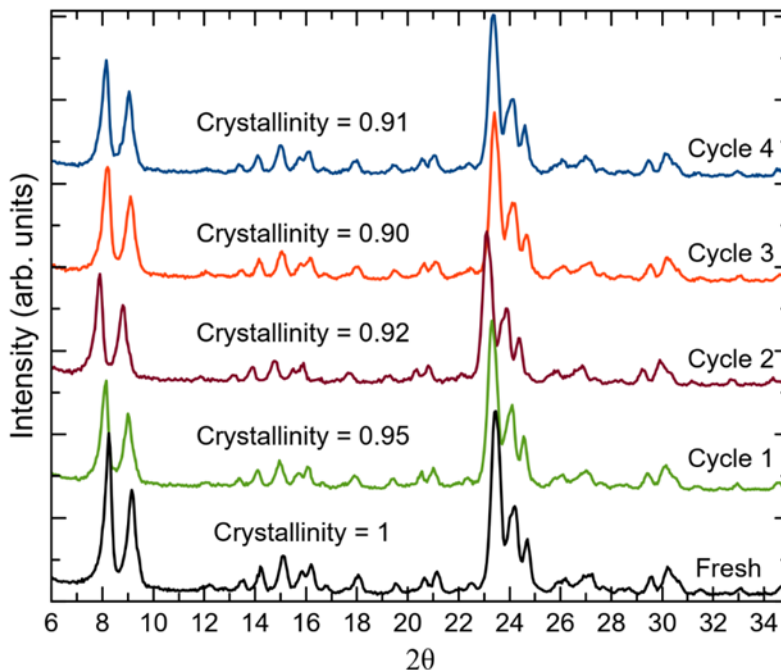


**Figure 4.** XRD patterns of fresh and regenerated ZSM-5. The corresponding degree of crystallinity is calculated using the ASTM Standard D5758 [47].

Used catalysts were tested using N<sub>2</sub> adsorption to evaluate effects on textural properties, Table 3 summarizes the results. After the first two uses, micropore area decreases by 21% and micropore volume by 13% relative to values measured for the native material. In subsequent cycles (three and four), these properties then remained constant. Micropore area decreases by 21% of the fresh catalyst over initial two uses before clearly stabilizing. Estimated external surface area followed a similar pattern, and the overall conclusion is that the catalyst shows no signs of

irreversible deactivation after 4 use-regeneration cycles. In comparison, Zaker et al. [20] reported that ZSM-5 surface area decreased by >40% after a single use under similar reaction conditions as used here, with the main difference being water loading (50 wt% vs. 15 wt% here).

| <b>Catalyst</b> | <b>Micropore Area [m<sup>2</sup>/g]</b> | <b>Micropore Volume [cc/g]</b> | <b>External Surface Area [m<sup>2</sup>/g]</b> | <b>Correlation Coefficient</b> |
|-----------------|---|--------------------------------|--|--------------------------------|
| Fresh           | 293                                     | 0.15                           | 60.2   | 0.99                           |
| Cycle 1         | 266                                     | 0.13                           | 49.8   | 0.99                           |
| Cycle 2         | 230                                     | 0.11                           | 40.5   | 0.98                           |
| Cycle 3         | 230                                     | 0.12                           | 41.3   | 0.99                           |
| Cycle 4         | 236                                     | 0.12                           | 36.6   | 0.98                           |

**Table 3.** Surface area properties of ZSM-5 after use in catalytic cracking reactions calculated using the t-plot method.

SEM was used to evaluate changes in particle morphology after each use-regeneration cycle. Figure 5 shows representative SEM images of the original material (Figure 5a) and catalyst after one (Figure 5b) and four use-regeneration cycles (Figure 5c). The native catalyst appears as an agglomerate of poorly defined nanoscale particles. One use-regeneration cycle results in a negligible change in the catalyst morphology, as shown in Figure 5b. After four use-regeneration cycles, the catalyst surface presents needle and flower-like features (Figure 5c). Maag et al. [23] previously described appearance of extensive needle-like features on the surface of ZSM-5 exposed to pure liquid or liquid-like supercritical water at the same temperature as used here for reaction, attributing their appearance to the ZSM-5 degradation process. In comparison with previous observations of ZSM-5 degradation made in pure water, the appearance of needle-like features is much less extensive in the presence of a reaction mixture containing 15 wt% water.

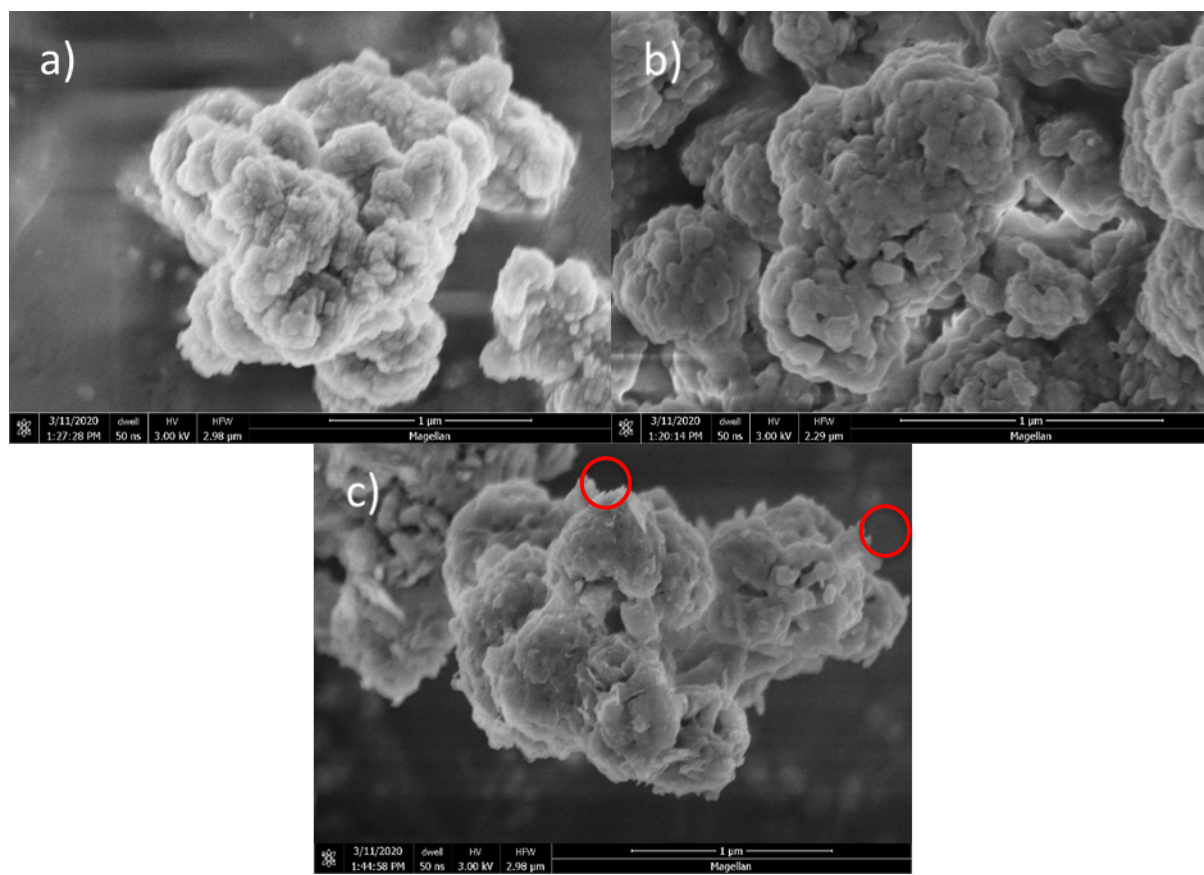


**Figure 5.** Scanning electron microscope images of a) fresh calcined catalyst, b) cycle 1 catalyst, and c) cycle 4 catalyst. Circled in red are examples of needle-like features present on the catalyst.

Brønsted acid sites (BAS) are the active sites for alkane cracking and aromatization reactions [[48-53] (Danuthai et al., Corma et al., Abbot, Tessennior et al., Bayense et al., Valle et al.)]. The aromatic yields reported after four use-regeneration cycles is indirect evidence of retained BAS density, since previous work showed that silicalite – which has no Brønsted acidity – failed to convert dodecane into aromatic products at similar conditions to those studied here [20]. To evaluate acid site chemistry in more detail, used-regenerated catalysts were studied using DRIFTS.[23, 54]. Figure 6 shows DRIFTS spectra obtained for the original catalyst material and catalyst after each of the four use-regeneration cycles. As expected, the original catalyst exhibits an intense band at approximately  $3600\text{ cm}^{-1}$  associated with the Al–OH stretch indicating

Brønsted acidity [55]. A second intense band at approximately  $3750\text{ cm}^{-1}$  can be attributed to the Si–OH stretch of the silanol group [55]. After the first cycle, the intensity of the feature attributed to Brønsted acidity decreases, and the intensity of a feature at  $3650\text{ cm}^{-1}$  increases. The feature at  $3650\text{ cm}^{-1}$  is attributable to extra-framework alumina (EFAL). Interestingly, the intensity of the silanol band may also decrease after the first use-regeneration cycle. In all subsequent cycles, both the BAS and EFAL feature are present, with the intensity of the BAS feature greater than that of the EFAL. The intensity of the silanol feature remains constant after decreasing after the first use-reuse cycle.

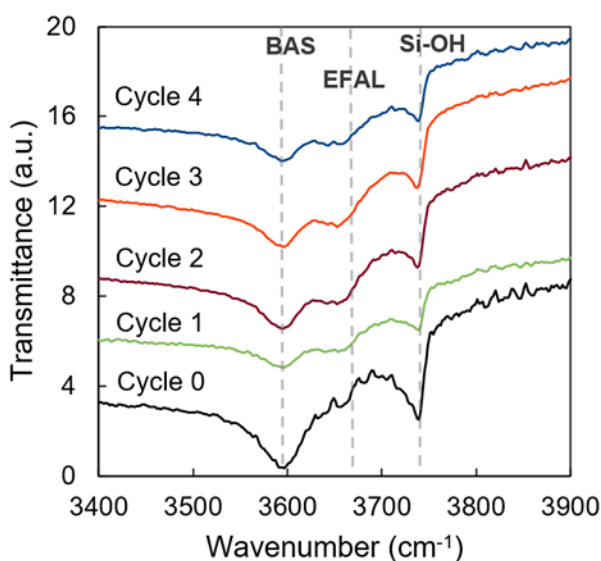


**Figure 6.** DRIFTS spectra of calcined ZSM-5 catalyst at increasing usage.

Conversion of BAS to EFAL is commonly observed as part of the dealumination process that removes acid sites from the zeolite framework [56]. Accordingly, the decreased intensity of the BAS feature and increased intensity of the EFAL feature after the first use-regeneration cycle is consistent with partial depletion of the original acid sites present on the catalyst. The persistence of the BAS feature after four use-regeneration cycles is consistent with retained acidity [55] and the observation of aromatic production (Figure 1). In comparison, Maag et al. [23] found that

exposure to pure supercritical water at 400 °C resulted in nearly complete disappearance of the BAS feature from the DRIFTS spectrum, corresponding with >70% reduction of BAS density measured by titration methods.

The response silanol feature shown in Figure 6 is worth further discussion. Silanol features are associated with defects in the zeolite lattice, [57] and are especially prominent at the surface.[58] Accordingly, the reduced intensity of the silanol band after the first use-regeneration cycle is consistent with the decreased surface area previously identified from measured N<sub>2</sub> isotherms. Stability of the silanol feature after subsequent use-regeneration cycles is therefore consistent with the aforementioned stability of textural properties.

The DRIFTS spectrum shows that BASs are present even after four uses of the catalyst. The importance of the BAS on the function of the catalyst necessitates further study [REF]. Isopropyl amine titration was performed in order to quantify the changes in BASs in the zeolite. The results can be seen in Table 4.

| <b>Catalyst</b> | <b>Bronsted Site Density (umol/g)</b> |
|-----------------|---------------------------------------|
| Cycle 0         | 617.06                                |
| Cycle 1         | 167.1                                 |
| Cycle 2         | 43.36                                 |
| Cycle 3         | 73.83                                 |
| Cycle 4         | 81.51                                 |

**Table 4.** Bronsted Acid Site properties of ZSM-5 catalyst measured through isopropyl amine titration.

The fresh catalyst (cycle 0) provides a baseline for the BAS density with the cycle 1 catalyst dropping in BAS density by 73%. Further use of the catalyst results in a final BAS density of 81.51 umol/g or approximately 13% of the fresh catalysts BAS density. The BAS density remains

relatively constant from cycle 2 to cycle 4 suggesting the BAS density has stabilized with further use. It is noticeable that the cycle 1 catalyst has neither the lowest surface area nor the lowest BAS density however it has the lowest aromatic production of all the catalyst tested.

In summary, four use-regeneration cycles of ZSM-5 in the presence of a minority water phase resulted in modest (<20%) reductions in activity and surface area, in parallel with some qualitative changes in surface morphology and BAS density revealed by DRIFTS. Prior work by Mo et al.[27] of palmitic acid cracking with a majority water component (66 wt%) did not report extensive characterization data, making difficult direct comparison with the results presented here. The most appropriate comparison is the work reported by Zaker et al. [20], performed in a reaction mixture consisting of 50 wt% water and 50 wt% dodecane. Compared with the previous work by Zaker et al. [20], using ZSM-5 in the presence of a minority water phase (15 wt%) resulted in much less degradation, indicating much greater potential for commercial use. Additionally, extending zeolite structural and acid site stability came in parallel with increased activity and without excessive coke formation. These positive findings motivate follow-on studies to examine the cracking and aromatization reaction in greater detail.

## **Reaction Pathway**

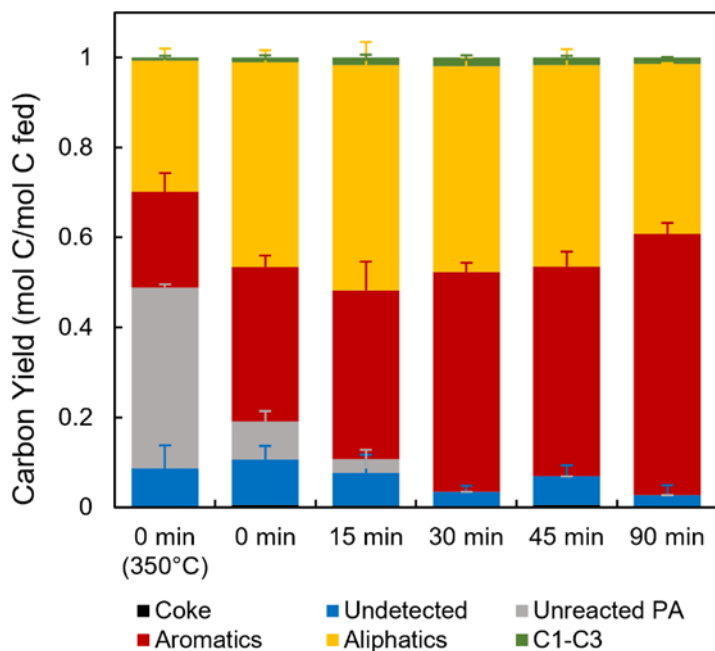
Experiments at both “hydrothermal” (SCW with no catalyst) conditions and catalytic conditions were conducted to better understand unique contributions to the reaction. Representative GC/FID spectra for hydrothermal and catalytic cracking products can be seen in SI-X. Hydrothermal conversion of PA (no catalyst, 15 wt% water,  $23 \pm 1$  MPa and 400 °C held for 30 minutes) resulted in complete conversion within detection limits a produced straight chain paraffins and relatively few straight chain olefins. Mass spectrometry showed signs of straight-

chain carboxylic acids, suggesting that decarboxylation and chain cracking are occurring simultaneously.

The carboxylic acid group is responsible for the high conversion of palmitic acid observed in SCW without catalyst, which is in line with work on hexyl-sulfide decomposition in SCW in which the alkane analog is unreactive [58]. Zaker et al.[20] found that in SCW-dodecane cracking with just SCW and with SCW, nitric acid, and silicalite framework, dodecane was unreactive. Therefore, it seems that SCW alone nor SCW with a strong acid present does not offer appropriate acid sites to imitate the carbocation isomerization and aromatization present with ZSM-5. From this and the product distribution, it seems that a radical pathway is responsible for decomposition without the presence of catalyst, with a rate which is not able to be neglected.

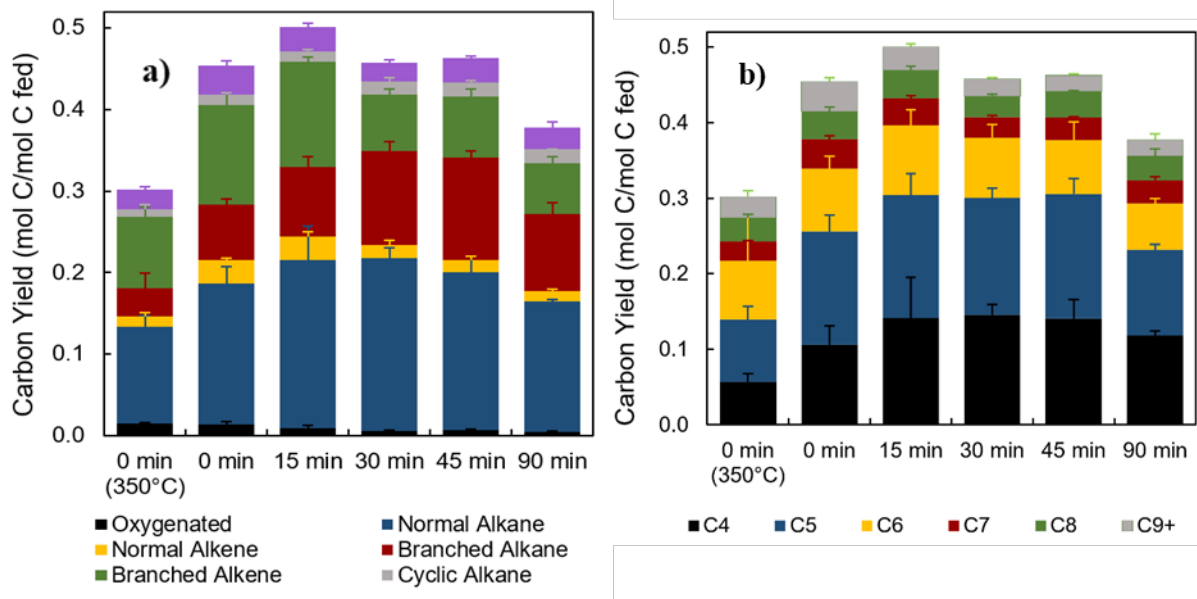
Prior research has identified the role of carbocation intermediates in cracking reactions with zeolites [40, 42]. Catalytic cracking of PA produced significant yields of aromatic compounds as well as of branched and cyclic paraffins and olefins, clearly demonstrating a catalytic pathway to isomerization and aromatization when juxtaposed against hydrothermal products. However, while the system has catalyst present, there is likely also radical thermal decomposition occurring outside of the catalyst.

Figure 7 shows the overall carbon yield breakdown of products over increasing temperature and reaction times. Aromatic yield increases with time even after PA is entirely converted. Combined with the decrease of aliphatics over the same time range, it is clear that aliphatics are being converted to aromatics.



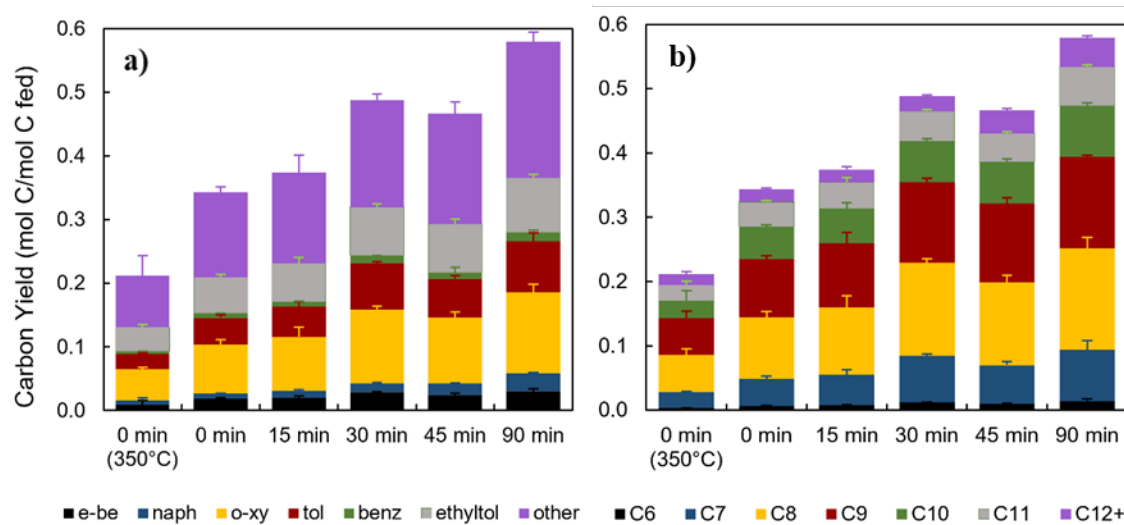
**Figure 7.** Overall carbon yield of all products at varying reaction times.

To search for a primary precursor to aromatic formation, aliphatic yields were analyzed in more detail in Figure 8.



**Figure 8.** Aliphatic yield by 1) compound type and b) carbon number.

Oxygenated aliphatics and branched alkenes are saturated by hydrogen from aromatization reactions over time, forming the trend of increasing alkanes and decreasing alkenes observed in Figure 8a. From 30 to 90 minutes, after complete PA conversion, aliphatic conversion decrease by  $80.5 \pm 16.6$  mmol C/mol C fed (mmol C yield), on par with the  $91.5 \pm 32.5$  mmol C yield increase in aromatics over the same duration; this decrease may be entirely attributed to a C4-C6 decrease of  $87.1 \pm 29.2$  mmol C yield from 30 to 90 minutes while C7-C8 increased by  $7.9 \pm 14.9$  mmol C yield. From this it likely seems straight-chain C4-C6 aliphatics are undergoing addition reactions to form aromatics and potentially also C7-C8 aliphatic isomers. This agrees with previous literature: Y. Ono et al [43] reacted pentanes over HZSM-5 to find that light olefins and C4 and C5 hydrocarbons acted as intermediates for aromatics while others have hypothesized that light olefins (C2-C4) serve as intermediates [43, 44]. While the data is sufficient to explain aromatic formation after complete PA conversion, the temporal aspect of these reactions suggest they are not the primary pathway as previous aromatic formation occurs much more rapidly.



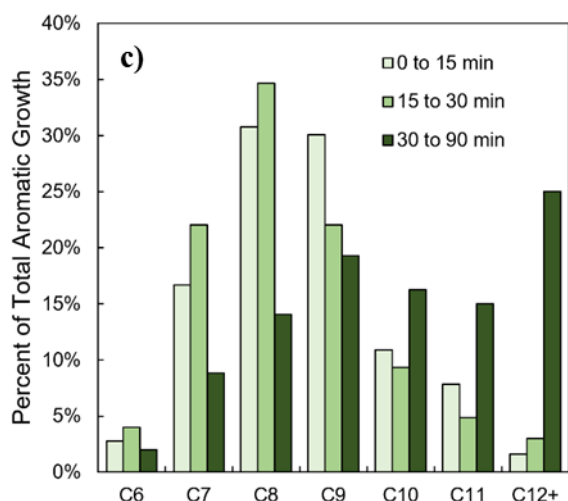


**Figure 9.** Aromatic yield by a) compound type, b) carbon number, and c) by increase between time points.

To better understand the reactions that may be taking place, an aromatic carbon balance was investigated in Figure 9. The aromatics which are formed between 0 to 30 minutes are not the primary aromatics being formed between 30 to 90 minutes, as can be seen in Figure 9c. From 15 to 30 minutes, C10+ aromatic increase by 20 mmol C yield while aromatics overall increase by 114 mmol C yield, representing 17% of the total increase, while C7-C8 aromatics represent 57%. From 30 to 90 minutes, C10+ aromatics constitute 56% of the aromatic carbon growth of 91 mmol C yield while C7-C8 constitute only 23%. Therefore, it appears that C4-C6 aliphatic additions and aromatization represent a slow, secondary pathway to aromatic formation separate from the primary pathway undertaken in the reaction while PA is present. The primary pathway appears to be related directly to the presence of PA due to the dramatic slow in aromatic production once PA is completely reacted, and therefore may be linked to intermediates formed as PA cracks on the surface of the catalyst. An alternative perspective may consider reduction of catalytic activity as coke forms on the catalyst surface reducing rates of aromatic production, but this is unlikely as

coking remains much lower than other studies have shown while maintaining catalytic activity.

Figure 10 details a proposed reaction pathway which encompasses this information.

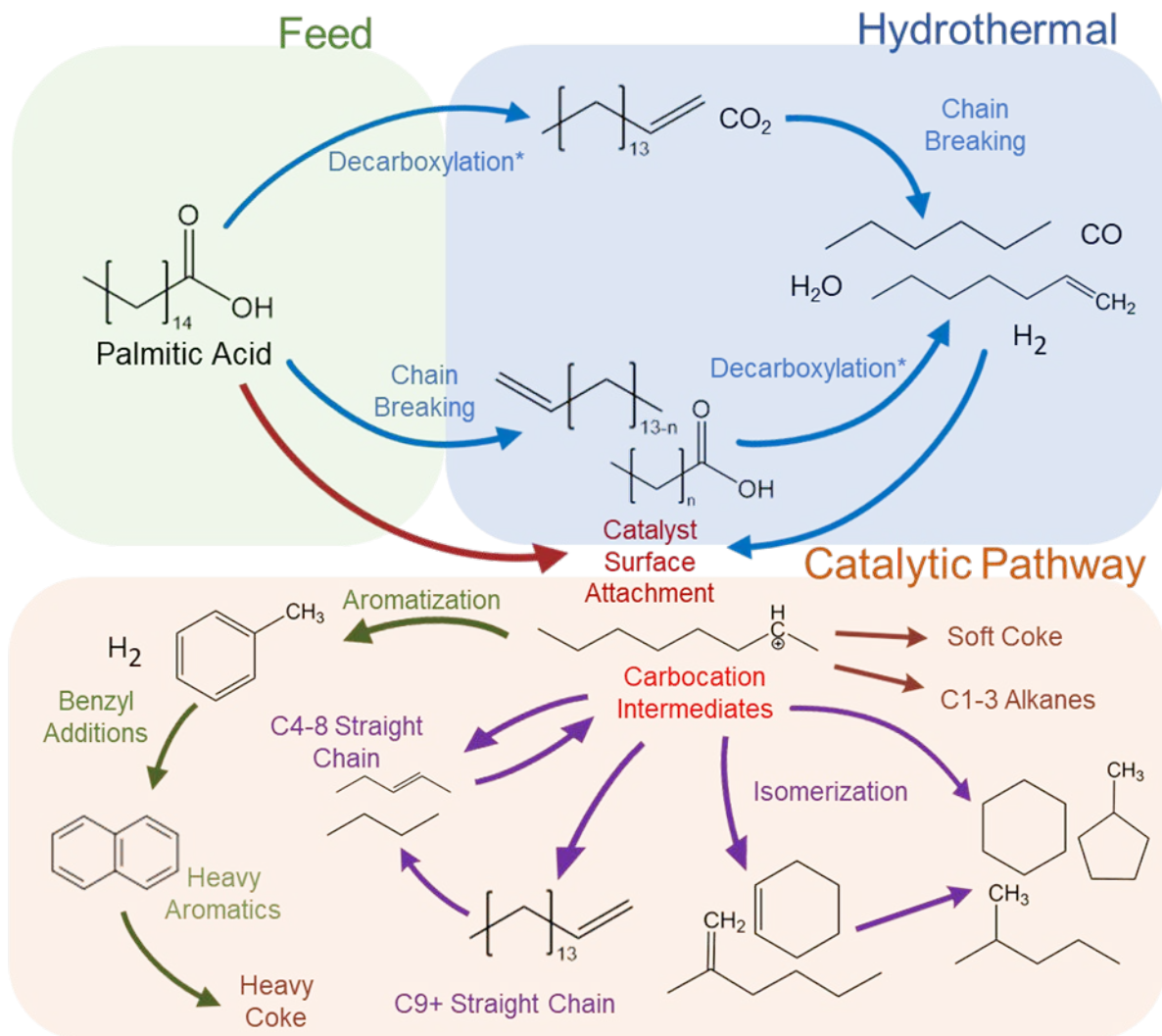


**Figure 10.** Overall reaction pathway showing classes of compounds formed through the cracking of palmitic acid (ignoring relative yields).

## Conclusion

Within this work, it has been shown that ZSM-5 can convert palmitic acid to desired aromatics and olefins at superior rates and with less catalyst loading, degradation, and coking than

previously found [27]. Added catalyst stability and coking is achieved through a lower water load which has been shown within previous works to decrease effects of coking and catalyst degradation [20, 21, 23]. Many findings in this work coincide with findings from previous works, including the importance of Brønsted acid sites for PA conversion and aromatization. Interestingly, it was found that catalyst activity decreased with the first reuse but increased slightly after subsequent uses. This can be attributed to catalyst degradation allowing access to pores previously blocked by prior degradation, increasing catalytic activity overall. It was demonstrated that ZSM-5 can be recycled for use at least four times retaining the vast majority of its activity and structural integrity. The reaction pathway of palmitic acid cracking was also investigated in this work. Chain cracking and decarboxylation reactions appear to be occurring through thermal radical pathways at rates which cannot be ignored when analyzing catalytic rates. While there does not appear to be a specific precursor to aromatic formation from product analysis at various reaction times/conversions, a secondary pathway appears to occur after complete conversion of PA from 30 to 90 minutes in which C4-6 addition and dehydroaromatization appears to be occurring to form a higher ratio of heavier aromatics (C10+). This work shows that having a minority weight content of water can be beneficial to the upgrading of an abundant fatty acid by increasing the catalyst's lifetime through coke suppression and minimal structural changes. Further work could explore the use of this strategy for the upgrading of other fatty acids and waste oils, and more work can be applied to further understanding catalytic and hydrothermal contributions to the reaction pathway.

## Acknowledgements

Jeffrey Page, Joseph Esposito, Douglas Theberge for working with me on this project.

Professor Michael Timko and Azadeh Zaker for guidance and help with analysis.

Sanket Sabnis and Wei Fan From University of Massachusetts Amherst for SEM images and analysis.

Professor Bond from Syracuse University with feedback on reaction pathway discussion.

Geoffrey Tompsett, Heather LeClerc, Cameron Armstrong for helping with lab work and data collection.

## References

1. Lund, H., *Renewable energy strategies for sustainable development*. Energy, 2007. **32**(6): p. 912-919.
2. Hussain, A., S.M. Arif, and M. Aslam, *Emerging renewable and sustainable energy technologies: State of the art*. Renewable and Sustainable Energy Reviews, 2017. **71**(Generic): p. 12-28.
3. Lin, Z., V. Nikolakis, and M. Ierapetritou, *Life cycle assessment of biobased p-xylene production*. Industrial and Engineering Chemistry Research, 2015. **54**(8): p. 2366-2378.
4. Harmsen, P.F.H., M.M. Hackmann, and H.L. Bos, *Green building blocks for bio-based plastics*. Biofuels Bioproducts and Biorefining, 2014. **8**(3): p. 306-324.
5. Cherubini, F., *The biorefinery concept: Using biomass instead of oil for producing energy and chemicals*. Energy Conversion and Management, 2010. **51**(7): p. 1412-1421.
6. Pellgino, J.L., *Energy and Environmental Profile of the U.S. Chemical Industry*, D. U.S. DOE: Washington, Editor. 2000.
7. Vlysidis, A., et al., *A techno-economic analysis of biodiesel biorefineries: Assessment of integrated designs for the co-production of fuels and chemicals*. Energy, 2011. **36**(8): p. 4671-4683.
8. Gudiyella, S., et al., *An experimental and modeling study of vacuum residue upgrading in supercritical water*. AIChE Journal, 2018. **64**(5): p. 1732-1743.
9. Botas, J.A., et al., *Catalytic conversion of rapeseed oil for the production of raw chemicals, fuels and carbon nanotubes over Ni-modified nanocrystalline and hierarchical ZSM-5*. Applied Catalysis B: Environmental, 2014. **145**: p. 205-215.
10. Emori, E.Y., et al., *Catalytic cracking of soybean oil using ZSM5 zeolite*. Catalysis Today, 2017. **279**: p. 168-176.

11. Ong, Y.K. and S. Bhatia, *The current status and perspectives of biofuel production via catalytic cracking of edible and non-edible oils*. Energy, 2010.
12. Katikaneni, S.P.R., J.D. Adjaye, and N.N. Bakhshi, *Studies on the Catalytic Conversion of Canola Oil to Hydrocarbons: Influence of Hybrid Catalysts and Steam*. Energy & Fuels, 1995. **9**(4): p. 599-609.
13. Katikaneni, S.P.R., J.D. Adjaye, and N.N. Bakhshi, *Catalytic conversion of canola oil to fuels and chemicals over various cracking catalysts*. The Canadian Journal of Chemical Engineering, 1995. **73**(4): p. 484-497.
14. Twaiq, F.A., A.R. Mohamed, and S. Bhatia, *Liquid hydrocarbon fuels from palm oil by catalytic cracking over aluminosilicate mesoporous catalysts with various Si/Al ratios*. Microporous and Mesoporous Materials, 2003. **64**(1): p. 95-107.
15. Zhang, H., et al., *Catalytic conversion of biomass-derived feedstocks into olefins and aromatics with ZSM-5: the hydrogen to carbon effective ratio*. Energy & Environmental Science, 2011. **4**(6): p. 2297-2307.
16. Bibby, D.M., et al., *Coke formation in zeolite ZSM-5*. 1986. p. 493-502.
17. Milina, M., et al., *Mesopore quality determines the lifetime of hierarchically structured zeolite catalysts*. Nature Communications, 2014. **5**(May).
18. Milina, M., S. Mitchell, and J. Pérez-Ramírez, *Prospectives for bio-oil upgrading via esterification over zeolite catalysts*. 2014. p. 176-183.
19. Taufiqurrahmi, N., A.R. Mohamed, and S. Bhatia, *Production of biofuel from waste cooking palm oil using nanocrystalline zeolite as catalyst: Process optimization studies*. Bioresource Technology, 2011.
20. Zaker, A., et al., *Evidence of heterogeneous catalytic activity of ZSM-5 in supercritical water for dodecane cracking*. Catalysis Today, 2018. **317**(May): p. 2-11.
21. Guerra, P., et al., *Analysis of coke formed during zeolite-catalyzed supercritical dodecane cracking: Effect of supercritical water*. 2020. p. 117330.
22. Zaker, A., et al., *Chemicals from heavy oils by ZSM-5 catalysis in supercritical water: Model compound and reaction engineering*. AIChE Journal. **n/a**(n/a): p. aic16237.
23. Maag, A.R., et al., *ZSM-5 decrystallization and dealumination in hot liquid water*. Physical Chemistry Chemical Physics, 2019.
24. Zhang, L., et al., *Factors that Determine Zeolite Stability in Hot Liquid Water*. Journal of the American Chemical Society, 2015. **137**(36): p. 11810-11819.
25. Ravenelle, R.M., et al., *Stability of zeolites in hot liquid water*. Journal of Physical Chemistry C, 2010.
26. Gardner, D.W., et al., *Insights into the Hydrothermal Stability of ZSM-5 under Relevant Biomass Conversion Reaction Conditions*. ACS Catalysis, 2015. **5**(7): p. 4418-4422.
27. Mo, N. and P.E. Savage, *Hydrothermal Catalytic Cracking of Fatty Acids with HZSM-5*. ACS Sustainable Chemistry & Engineering, 2014. **2**(1): p. 88-94.
28. Schreiber, M.W., et al., *Hydrodeoxygenation of fatty acid esters catalyzed by Ni on nano-sized MFI type zeolites*. Catalysis Science & Technology, 2016. **6**(22): p. 7976-7984.
29. Ma, B., et al., *Interconnected hierarchical HUSY zeolite-loaded Ni nano-particles probed for hydrodeoxygenation of fatty acids, fatty esters, and palm oil*. Journal of Materials Chemistry A, 2016. **4**(29): p. 11330-11341.
30. Chen, D., K. Moljord, and A. Holmen, *A methanol to olefins review: Diffusion, coke formation and deactivation on SAPO type catalysts*. Microporous and Mesoporous Materials, 2012. **164**: p. 239-250.
31. Kim, J., M. Choi, and R. Ryoo, *Effect of mesoporosity against the deactivation of MFI zeolite catalyst during the methanol-to-hydrocarbon conversion process*. Journal of Catalysis, 2010. **269**(1): p. 219-228.

32. Duan, P., et al., *Catalytic upgrading of pretreated algal bio-oil over zeolite catalysts in supercritical water*. Biochemical Engineering Journal, 2016. **116**: p. 105-112.
33. Tamunaidu, P. and S. Bhatia, *Catalytic cracking of palm oil for the production of biofuels: Optimization studies*. Bioresource Technology, 2007. **98**(18): p. 3593-3601.
34. Liu, M., et al., *Upgrading of palmitic acid and hexadecanamide over Co-based catalysts: Effect of support (SiO<sub>2</sub>,  $\gamma$ -Al<sub>2</sub>O<sub>3</sub> and H-ZSM-22)*. Catalysis Communications, 2019.
35. He, P. and A.F. Ghoniem, *A Group Contribution Pseudocomponent Method for Phase Equilibrium Modeling of Mixtures of Petroleum Fluids and a Solvent*. Industrial & Engineering Chemistry Research, 2015. **54**(35): p. 8809-8820.
36. Perkins, G., R.E. Laramy, and L.D. Lively, *Flame Response in the Quantitative Determination of High Molecular Weight Paraffins and Alcohols by Gas Chromatography*. Analytical Chemistry, 1963. **35**(3): p. 360-362.
37. McHugh, M. and V. Krukoniš, *Supercritical fluid extraction: practice and purpose*. Second ed. 2013: Elsevier.
38. Wagner, W. and A. Pruß, *The IAPWS Formulation 1995 for the Thermodynamic Properties of Ordinary Water Substance for General and Scientific Use*. Journal of Physical and Chemical Reference Data, 2002. **31**(2): p. 387-535.
39. Santos, M.R., et al., *Catalytic cracking of palmitic and oleic acids pre-adsorbed on  $\gamma$ -alumina*. Catalysis Today, 2019(May 2018): p. 1-6.
40. Class, C.A., et al., *Detailed kinetic model for hexyl sulfide pyrolysis and its desulfurization by supercritical water*. Physical Chemistry Chemical Physics, 2019. **21**(20): p. 10311-10324.
41. Kotrel, S., H. Knözinger, and B.C. Gates, *The Haag-Dessau mechanism of protolytic cracking of alkanes*. Microporous and Mesoporous Materials, 2000.
42. Sirokman, G., Y. Sendoda, and Y. Ono, *Conversion of pentane into aromatics over ZSM—5 zeolites*. Zeolites, 1986. **6**(4): p. 299-303.
43. Scurrall, M.S., *Factors affecting the selectivity of the aromatization of light alkanes on modified ZSM-5 catalysts*. Applied Catalysis, 1988. **41**: p. 89-98.
44. Zapata, P.A., et al., *Silylated hydrophobic zeolites with enhanced tolerance to hot liquid water*. 2013. p. 82-97.
45. Nandiwale, K.Y., et al., *Catalytic upgrading of renewable levulinic acid to ethyl levulinate biodiesel using dodecatungstophosphoric acid supported on desilicated H-ZSM-5 as catalyst*. 2013. p. 90-98.
46. ASTM, *D5758-01* 2011, ASTM International p. 3-5.
47. Corma, A., et al., *The role of different types of acid site in the cracking of alkanes on zeolite catalysts*. Journal of Catalysis, 1985. **93**(1): p. 30-37.
48. Danuthai, T., et al., *Conversion of methylesters to hydrocarbons over an H-ZSM5 zeolite catalyst*. Applied Catalysis A: General, 2009. **361**(1-2): p. 99-105.
49. Abbot, J., *Role of Brønsted and Lewis acid sites during cracking reactions of alkanes*. Applied Catalysis, 1989. **47**(1): p. 33-44.
50. Bayense, C.R., A.J.H.P. van der Pol, and J.H.C. van Hooff, *Aromatization of propane over MFI-gallosilicates*. Applied Catalysis, 1991. **72**(1): p. 81-98.
51. Tessonnier, J.-P., et al., *Methane dehydro-aromatization on Mo/ZSM-5: About the hidden role of Brønsted acid sites*. Applied Catalysis A: General, 2008. **336**(1-2): p. 79-88.
52. Valle, B., et al., *Hydrothermally stable HZSM-5 zeolite catalysts for the transformation of crude bio-oil into hydrocarbons*. Applied Catalysis B: Environmental, 2010. **100**(1-2): p. 318-327.
53. Kumar, V.V., et al., *Role of Brønsted and Lewis acid sites on Ni/TiO<sub>2</sub> catalyst for vapour phase hydrogenation of levulinic acid: Kinetic and mechanistic study*. Applied Catalysis A: General, 2015. **505**: p. 217-223.

54. Datka, J., et al., *Physicochemical and Catalytic Properties of HZSM-5 Zeolites Dealuminated by the Treatment with Steam*. The Journal of Physical Chemistry, 1996. **100**(34): p. 14451-14456.
55. Loeffler, E., et al., *Study of different states of nonframework aluminum in hydrothermally dealuminated HZSM-5 zeolites using diffuse reflectance i.r. spectroscopy*. Zeolites, 1990. **10**(4): p. 266-271.
56. Ye, Y., et al., *Influence of Silanol Defects of ZSM-5 Zeolites on Trioxane Synthesis from Formaldehyde*. Catalysis Letters, 2020. **150**(5): p. 1445-1453.
57. Barbera, K., et al., *Structure–deactivation relationship for ZSM-5 catalysts governed by framework defects*. Journal of Catalysis, 2011. **280**(2): p. 196-205.
58. Kido, Y., et al., *Supercritical Water Desulfurization of Organic Sulfides Is Consistent with Free-Radical Kinetics*, Energy Fuels, 2013. **27**(10): p. 6108-6117.
59. Wisniewski, A., et al., *Biofuels from waste fish oil pyrolysis: Chemical composition*. Fuel, 2010. **89**(3): p. 563-568.

## Appendix

### <sup>1</sup>H NMR of heavy oil products

To analyze “heavy” oil-phase products, referring to compounds which are non-volatile within the parameters of our gas chromatography analysis, we performed ambient evaporation-to-dryness within a fume hood for 3 weeks. The resulting oil phases were then analyzed with proton NMR, the results of which can be seen in Figures A1 and A2.

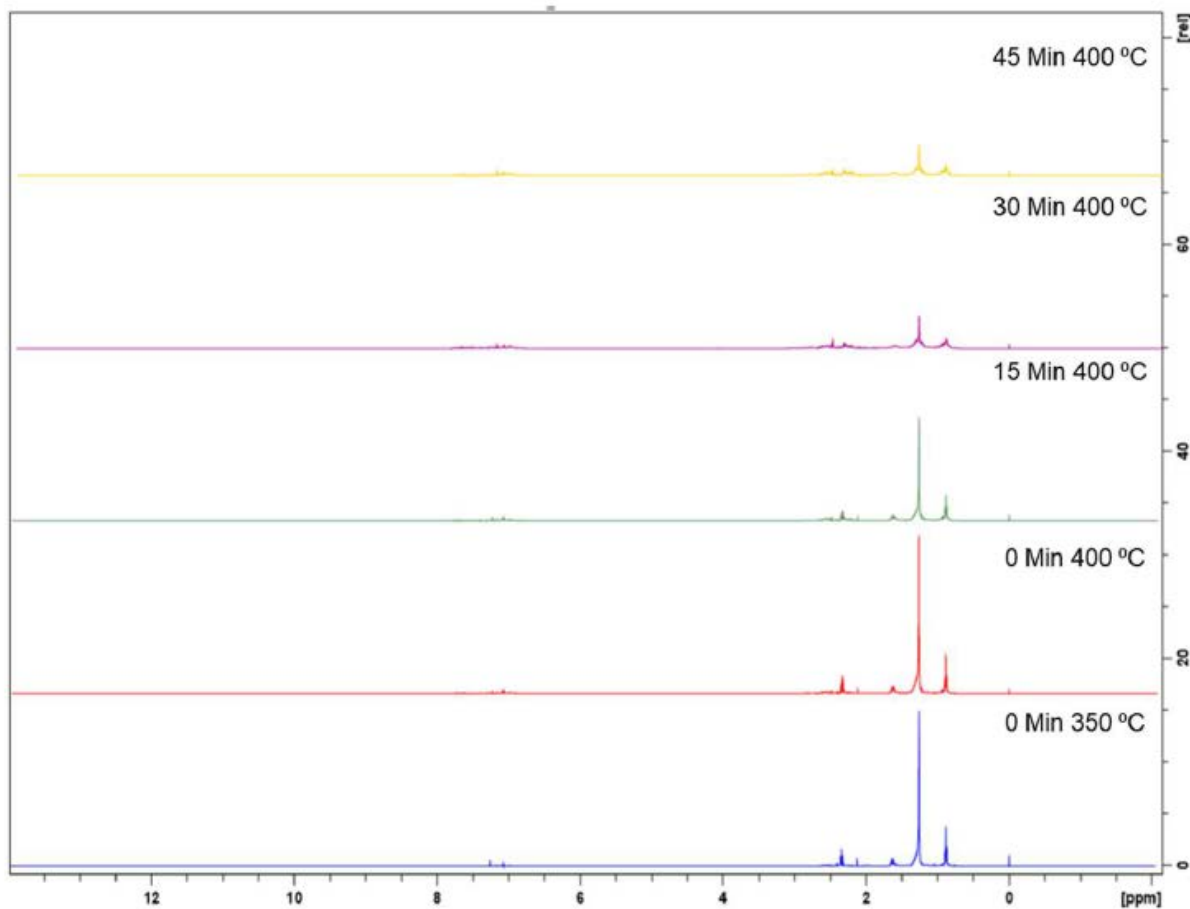


**Figure A1.** Proton NMR data for “heavy oil” products, acquired through evaporation-to-dryness for 3 weeks inside of a fume hood of product oil phase. Integrations of peaks can be found in Figure A2 below.

Integration was performed on the NMR shifts found in graph A1. Each peak represents a hydrogen on a different functional group. For the purposes of this study the shifts between 0.5 and 2.5 ppm are consider aliphatic hydrogen, shifts between 2.5 and 3 ppm are consider aliphatic hydrogen attached to an aromatic molecule and shifts between 7 and 9 ppm are considered aromatic [59]. The area of the aliphatic peaks and the area aromatic peaks were divided by the total area to get the area fraction which is plotted in Figure A2. It is noteworthy that no peaks were found in the 11-12 ppm range which is generally expected for oxygenated compounds.

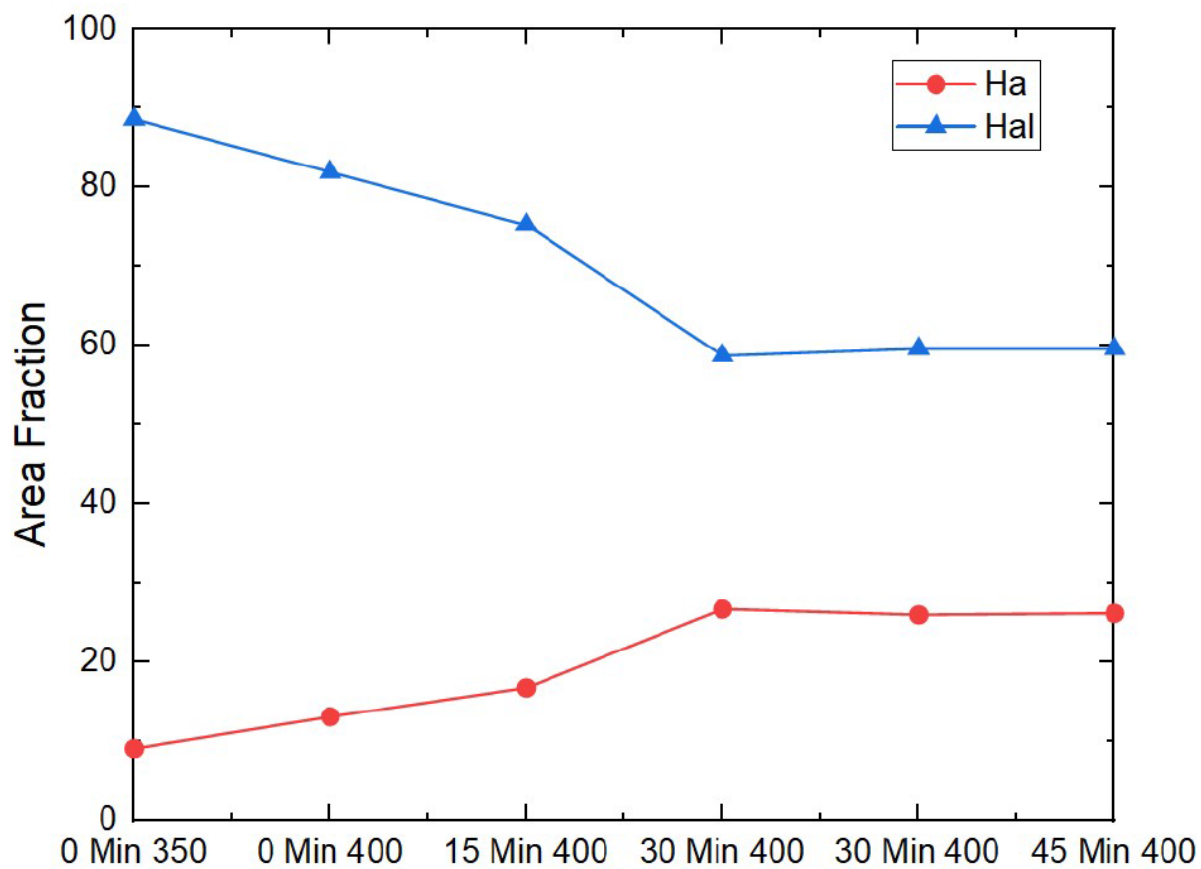


**Figure A2.** NMR peak area of aliphatic and aromatic hydrogen divided by the total area of all the peaks plotted at each reaction time point. 'Hal' represents aliphatic hydrogen and 'Ha' represents aromatic hydrogen.